J. Phys. Chem. A

Infrared Spectroscopy of Gold Carbene Cation ($AuCH_2^+$): Covalent or Dative Bonding?

P. B. Armentrout,[†,] Brandon C. Stevenson,[†] Fan Yang,[†] Frank J. Wensink,[‡] Olga V. Lushchikova,[‡] and Joost M. Bakker[‡]*

[†]Department of Chemistry, University of Utah, 315 South 1400 East, Room 2020, Salt Lake City, Utah 84112, USA

[‡]Radboud University, Institute for Molecules and Materials, FELIX Laboratory, Toernooiveld 7, 6525 ED Nijmegen, The Netherlands

Abstract. The present work explores the structure of the gold carbene cation, $AuCH_2^+$, using infrared multiple photon dissociation (IRMPD) action spectroscopy and density functional theory (DFT). Unlike several other 5d transition metal cations (M^+ = Ta^+, W^+, Os^+, Ir^+, and Pt^+) that react with methane by dehydrogenation to form MCH_2^+ species, gold cations are unreactive with methane at thermal energies. Instead, the metal carbene is formed by reacting atomic gold cations formed in a laser ablation source with ethylene oxide (cC_2H_4O) pulsed into a reaction channel downstream. The resulting $[Au,C,2H]^+$ product photofragmented by loss of H_2 as induced by radiation provided by the Free-Electron Laser for IntraCavity Experiments (FELICE) in the 300 − 1800 cm^{-1} range. Comparison of the experimental spectrum, obtained by monitoring the appearance of AuC^+, and DFT calculated spectra leads to identification of the ground state carbene, $AuCH_2^+$ ($^1A_1$) as the species formed, as previously postulated theoretically. Unlike the covalent double bonds formed by the lighter, open shell 5d transition metals, the closed shell Au^+ (^1S, $5d^{10}$) atom binds to methylene by donation of a pair of electrons from CH_2($^1A_1$) into the empty 6s orbital of gold coupled with π backbonding, i.e., dative bonding, as explored computationally. Contributions to the AuC^+ appearance spectrum from larger complexes are also considered and H_2CAu^+(c-C_2H_4O) seems likely to contribute one band observed.

Introduction

It would be of great technological interest to develop economical and efficient catalysts for the activation of methane, a major component of natural gas.[1-2] Direct conversion into liquid fuels and commodities such as methanol, ethene, or ethane, would retain the energy content of the hydrocarbon while permitting much easier transport. Despite the interest in such catalysts, progress has been slow and might be assisted by understanding factors that permit CH bond activation. By eliminating the complexities of solvent, stabilizing ligands, and solid-phase supports, gas-phase studies may provide a means for elucidating the intrinsic activation properties of metals.[3-4] Such gas-phase work also yields benchmark information that can be directly compared with theory, thereby guiding theoretical studies of more complex systems. Early work by Irikura and Beauchamp showed that methane was activated by a number of 5d transition metal cations (Ta^+, W^+, Os^+, Ir^+, and Pt^+) at room temperature, yielding the dehydrogenation products, $[M,C,2H]^+ + H_2$.[5] Survey work has subsequently shown that none of the other third-row, none of the first-row, and only Zr^+ of the second-row transition metal cations activate methane at room temperature.[6] A host of additional studies have confirmed these results,{Allison, 1986 #3920}{ Squires, 1987 #676;Aristov, 1987 #1379;Sunderlin, 1988 #1599;Schultz, 1988 #1468;Georgiadis, 1988 #1600;Sunderlin, 1989 #781;Russell, 1989 #887;Eller, 1991 #686;Chen, 1995 #845;Armentrout, 1996 #282;Haynes, 1995 #1606;Haynes, 1996 #864;Chen, 1997 #846;Armentrout, 1999 #281;Sievers, 2000 #835;Armentrout, 2003 #818;Liu, 2005 #1357;Armentrout, 2006 #1504;Shayesteh, 2009 #2268;Roithová, 2010 #2269;Schwarz, 2011 #2451;Irikura, 1989 #1514;Buckner, 1989 #850;Irikura, 1991 #613;Irikura, 1991 #896;Zhang, 2001 #586;Armentrout, 2006 #1363;Li, 2006 #1380;Parke, 2007 #1490;Armentrout, 2013 #2511;Armentrout, 2017 #3314} and demonstrated that the Zr^+ reaction is slightly endothermic and therefore inefficient.[23] Guided ion beam studies have extended this work to higher collision energies, thereby providing quantitative information about the reactivity and energetics of these reactions across the periodic table.[13, 29-38] More recently, it has been reported that cationic gold clusters will activate methane,[39] although initial reports of catalytic activity to form ethene have been proven erroneous.[40]

None of these studies provide any structural information about the species formed and therefore, for many years, theory has constituted the only structural information available. In the earliest work, Irikura and Goddard found that the 5d transition metal $[M,C,2H]^+$ species all had MCH_2^+ carbene structures having C_{2v} symmetry.[41] Simon et al. later calculated that carbene and carbyne hydride ($HMCH^+$) structures of $[W,C,2H]^+$ were close in energy,[42] and that the carbene exhibited agostic interactions. The latter distort the carbene to C_s symmetry and occur for early transition metals because electrons in a C-H bond donate into an empty metal d-orbital.[43-45]

Recently, these theoretical predictions were tested experimentally by infrared multiple photon dissociation (IRMPD) spectroscopic studies of the $[M,C,2H]^+$ species (and their deuterated counterparts).[46-48] As originally suggested by Simon et al., the ground states of $[Ta,C,2H]^+$ and $[W,C,2H]^+$ were found to have carbene structures distorted by agostic interactions. In agreement with Irikura and Goddard, $[Pt,C,2H]^+$ had the classic C_{2v} symmetry carbene structure, whereas $[Os,C,2H]^+$ had the carbyne hydride structure. $[Ir,C,2H]^+$ showed bands indicating a mixture of both $HIrCH^+$ (dominant) and $IrCH_2^+$ structures. The interpretation of $[Pt,C,2H]^+$ and $[Ir,C,2H]^+$ spectra was complicated by additional bands,[46] identified as overtones in later work on the perdeuterated isotopologues.[47] These latter systems also demonstrated the importance of the rotational substructures of the vibrational bands, evident in all five metal systems. These were the first observations of rotational structure in IRMPD spectra for covalently bound systems, although IR photodissociation spectra of weakly bound species had also exhibited such structure.[49] Likewise, the interactions of Au_2^+, Au_3^+, and Au_4^+ with methane have been probed using IRMPD spectroscopy, with methane adducts dominating the structures found but clear evidence for methyl hydride species as well.[50]

One important aspect of these studies and one retained in the present work is that they are enabled by the Free Electron Laser for Intra-Cavity Experiments (FELICE) beamline. Indeed, we have shown that obtaining IRMPD spectra of $[Pt,C,2H]^+$ and $[Pt,C,2D]^+$ is *not* possible using the extracavity output of the normal FELIX beam lines.[51] This is attributed to a combination of relatively high internal energy thresholds towards fragmentation and to the low state density of

these four-atom $[M,C,2H]^+$ systems. Notably, these are among the smallest molecules successfully studied by IRMPD action spectroscopy,[52-54] and the only ones examined over such an extensive IR spectral range. Generally, IRMPD requires that molecules absorb a photon in a specific vibrational coordinate, rapidly followed by energy redistribution into the other vibrational modes via intramolecular vibrational redistribution (IVR),[55-56] freeing up the acceptor mode for subsequent absorption. Clearly, the vibrational state density (the 'bath') available in a four-atom system is quite low, sufficiently so that the IVR rate is slow and limits how efficiently multiple IR photons can be absorbed in a single vibrational well. The FELICE beamline overcomes this limitation by brute force, as the intracavity arrangement allows about 100 times higher pulse energies.

In the present study, we extend our work to structurally characterize $[M,C,2H]^+$ species of gold, another 5d transition metal cation that does not exothermically dehydrogenate methane. Rather, $[Au,C,2H]^+$ species are formed by reaction of laser ablated Au^+ with ethylene oxide, c-C_2H_4O, as previously demonstrated by Metz and co-workers.[57] In their spectroscopic study, they irradiated the $[Au,C,2H]^+$ cation with light between 290 and 330 nm (4.27 – 3.76 eV), observing dissociation into both AuC^+ and Au^+ in a 1.4:1.0 ratio. A common threshold for production of both fragment ions of 322 nm indicates upper limits of 3.86 ± 0.03 eV for both $D_0(Au^+\text{-}CH_2)$ and $D_0(AuC^+\text{-}H_2)$. In subsequent work, Li et al. used guided ion beam tandem mass spectrometry to examine the endothermic reactions of Au^+ with methane (and perdeuterated methane).[38] The dominant product at lower collisions energies was $[Au,C,2H]^+$, formed with a threshold that indicated $D_0(Au^+\text{-}CH_2)$ = 3.70 ± 0.07 eV, in agreement with the upper limit from Metz and co-workers. Neither of these values agrees with a lower limit of 4.12 eV suggested by Chowdhury and Wilkins,[58] although this was later reinterpreted as >4.01 eV.[41] This latter theoretical work calculated a $Au^+\text{-}CH_2$ bond energy of 3.35 eV, which was empirically corrected to 3.86 ± 0.30 eV.[41] Subsequent theoretical calculations have obtained bond energies of 3.76,[59] 3.92,[60] and 3.69[38] eV, all in reasonable agreement with the experimental value. All theoretical studies also agree that the ground state of $AuCH_2^+$ is $^1A_1$ in which the $^1A_1$ excited state of CH_2 donates its lone pair of

electrons into the empty 6s orbital of ground state Au^+ (^1S, $5d^{10}$). Irikura and Goddard characterized this as a nearly pure dative bond augmented by π backbonding of the occupied 5dπ electrons on Au^+ into the empty b_1 orbital of CH_2 ($^1A_1$). Until the present report, experimental confirmation of this structure has yet to be achieved.

Experimental and Computational Methods

Experimental Details

A molecular beam apparatus connected to the first beamline of FELICE, as described in detail elsewhere,[54, 61] was used for the IRMPD action spectroscopy experiments. Atomic gold cations were created using a Smalley-type laser ablation source, [62-63] with a 0.1 mm thick Au foil spot welded onto a stainless steel rod as the ablation target. This target, which was rotated and translated, was irradiated with the second harmonic of a loosely focused, pulsed Nd:YAG laser (532 nm), yielding a plasma constrained in a 3 mm diameter × 60 mm long channel by helium injected into the channel via a pulsed valve (General Valve Series 9). A second pulsed valve was used to inject ethylene oxide (c-C_2H_4O) (5% in He) into the channel approximately 50 mm downstream from the laser ablation point. Gold cations reacted inefficiently with c-C_2H_4O to form $[Au,C,2H]^+$ (*m/z* 211) as the dominant product ion, surmised by the large ratio of Au^+ to $[Au,C,2H]^+$, see Supporting Figure S1. Smaller amounts of species such as $[Au,2C,2H]^+$ (*m/z* 223), $[Au,2C,4H]^+$ (*m/z* 225), $[Au,C,2H,O]^+$ (*m/z* 227), $[Au,2C,2H,O]^+$ (*m/z* 239), $[Au,2C,4H,O]^+$ (*m/z* 241), and ethylene oxide adducts of these species were also formed. Supporting Figure S1 shows a complete mass spectrum.

At the end of the channel, the gas pulse expanded into vacuum forming a molecular beam, which was collimated by an electrically grounded skimmer (2 mm diameter) and a horizontal slit aperture (8 × 0.45 mm). The molecular beam then entered the intracavity region at an angle of 35° with respect to the (horizontal) FELICE IR laser beam. The present experiments examined IR radiation in the 300 – 1800 cm^{-1} spectral range, where the FELICE macropulse (typical duration of 7 μs) consisted of ps-long micropulses separated by 1 ns. The radiation was near transform-

limited, with a spectral width set to $\sigma \sim 0.3\%$ of the central frequency (thus, a full-width at half-maximum (fwhm) of ~7 cm^{-1} at 1000 cm^{-1}); typical macropulse energies were 0.6-0.8 J. The molecular beam and the IR light interacted for several μs before all ions were pulse extracted into a (vertical) reflectron time-of-flight (RETOF) mass spectrometer (Jordan TOF Products, Inc.; mass resolution, $M/\Delta M \approx 1700$). A 400 Msample/s 100 MHz digitizer (Acqiris DP310) recorded transients from the multichannel plate (MCP) detector. The molecular beam was pulsed at twice the rate of FELICE, which allows the acquisition of reference mass spectra. This operation permits corrections for long-term source fluctuations and the unambiguous determination of which fragments are generated by irradiation with FELICE (see Figure S1 for an example).

Gold has only one stable isotope at 197 amu. Spectra shown were obtained by monitoring fragmentation into AuC^+ and correcting for the small amounts of AuC^+ present without laser irradiation. Experimental IRMPD spectra for $[Au,C,2H]^+$ were constructed by calculating the fragmentation yield, which equals $-\ln[P/(P + F)]$, where F and P are the fragment and precursor ion intensities, respectively, and correcting it for the IR macropulse energy. Possible fragmentation to the free Au^+ product by loss of CH_2 was not included in the yield calculations because a substantial signal of the atomic Au^+ bare metallic cation was present in the molecular beam (see Figure S1).

Metz and coworkers previously observed identical thresholds for H_2 and CH_2 loss of 3.86 ± 0.03 eV (upper limits to the true thermochemistry),[57] while subsequent experimental thermochemistry indicates the CH_2 loss channel requires 3.70 ± 0.07 eV.[38] Notably, theoretical calculations suggest that loss of H (forming $[Au,C,H]^+$) requires 4.6 eV, consistent with fragmentation into this channel not being observed both here and by Metz and coworkers. As for most other 5d transition metals,[29, 31] decomposition by loss of H_2 is relatively low in energy because the metal carbide bond energies are enhanced by π backbonding using occupied 5dπ orbitals.[34] These energetics indicate that the minimum number of IR photons needed for decomposition are >60 and >19 at 500 and 1600 cm^{-1}, respectively. Generally, more photons are

needed for the fragmentation rate to be high enough to observe signal within the 10 – 100 μs experimental time window.

For $[Au,C,2H]^+$, spectra were obtained only in-focus (maximum fluence), whereas no photodissociation was observed out-of-focus. These two instrumental conditions refer to translating the entire experimental apparatus along the FELICE laser beam, which reduces the fluence by up to a factor of 30 at a maximum translation of 300 mm out of focus of the FELICE optical beam with its 55 mm Rayleigh range. The range of fluences in the focus extended from 40 J/cm^2 at 300 cm^{-1} to 200 J/cm^2 near 1400 cm^{-1}, with estimated peak power densities ranging from 7×10^8 to 2×10^{10} W/cm^2.

Computational Details

Density functional theory (DFT) calculations were performed using the Gaussian 16 suite of programs [64] for various possible structures of $[Au,C,2H]^+$ and other related species. Theoretical IR spectra were computed for comparison with the observed IRMPD experimental spectrum. Computations utilized the B3LYP hybrid density functional[65-66] and def2-TZVPPD basis set, which is a balanced triple-zeta basis set with two polarization functions and one diffuse function on all elements with an all-electron basis set for C and H and a small-core effective core potential (ECP) for gold.[67] The gold basis set employed here explicitly includes the 5s, 5p, 6s, 6p, and 5d electrons. A similar approach was taken in previous spectroscopic studies of $[M,C,2H]^+$ for M^+ = Ta^+, W^+, Os^+, Ir^+, and Pt^+.[46-48] The present calculations utilize a more advanced basis set than previous work examining all species formed in the reaction of Au^+ with CH_4 (B3LYP/HW+).[38] In the determination of relative energies, vibrational frequencies used for zero-point energy calculations were scaled by 0.9885[68] to account for anharmonicities (whose accuracy is further demonstrated below).

Experimental and theoretical spectra were compared after scaling the harmonic frequencies of the latter by a global scaling factor of 0.975 to account for anharmonicity and other multiple photon effects. This factor provides reasonable agreement with the present experiments and is

similar to scaling factors used previously for other 5d $[M,C,2H]^+$ species (0.939 – 0.980).[46-48] When rotational substructure is not included, the theoretical spectra were convoluted using a 30 cm^{-1} fwhm Gaussian line shape function (as utilized previously for the late transition metals, Os, Ir, and Pt).[46-48] Previous work included anharmonic frequency calculations for the Ta, W, Os, Ir, and Pt systems and yielded only small shifts in the calculated resonances.[46, 48] A similar result is obtained here. Because relative band positions vary by less than 10 cm^{-1}, both anharmonic and harmonic frequencies provide the same comparisons to the data when scaled appropriately. For consistency with our previous work, the scaled harmonic frequencies are used below for comparison to the data.

Rotational Contours

Our previous work on the $[M,C,2D]^+$ systems where $M^+ = Ta^+$, W^+, Os^+, Ir^+, and Pt^+ showed strong evidence for the influence of rotational broadening.[47-48] These small ions have rotational constants that are on the same order as the spectral bandwidth of the exciting laser. Depending on the temperature, a substantial population of rotational sublevels, each giving rise to individual rovibrational transitions, could result in a substantially broadened vibrational band. Although the experiments are performed near room temperature, the true temperature of the ions is unknown. The expansion into vacuum could cool the ions, but it is unclear how efficient this cooling is and the ions start out being warmed by the energy released in the exothermic reaction. Thus, an appreciable population of excited rotational sublevels contributed to broadening of the bands in these systems.

Analogous to that work, the present work includes rotational contours for each predicted vibrational band simulated using dedicated software to diagonalize the pure rotational Hamiltonians.[69] The rotational transitions were simulated by convoluting the transition dipole moments originating from a wide range of $J_{Ka,Kc}$ states with a single temperature Boltzmann state distribution, with no change in the rotational constants between the vibrational ground and excited states (an assumption that could lead to discrepancies with the actual spectrum). The rotational

temperature was chosen to be 77 K, which provides a reasonable match between experimental and simulated spectra (as seen below). All ro-vibrational transitions were assumed to be pure a-, b- or c-type, which should be exact for symmetric ground state species. Detailed information needed for these analyses are included in the Supporting Table S1 and Supporting Figure S2. The distribution of rotational transitions that resulted was then shifted in frequency by the (scaled) harmonic frequency of the associated vibrational band, and convoluted with a Gaussian lineshape function (width σ = 0.3% of the central frequency), which represents the FELICE spectral profile.

The qualitative character of the various transitions can also be considered. a-type transitions are closest to a classic diatomic molecular spectrum with transitions for ΔK_a=0, ΔK_c=±1, and, because the B and C rotational constants are very similar, showing separated P and R branches, along with contributions from a weak Q branch (strictly forbidden for a diatomic, but not for polyatomics). In contrast, b- and c-type are much more complicated because of a variety of distinct ΔK_a and ΔK_c transitions (ΔK_a=±1, ΔK_c=0,±2 for c-type; ΔK_a=±1, ΔK_c=-+1for b-type), which each have P, Q, and R branches that do not line up. Thus, the rotational substructure is a fairly spread out and complicated superposition of P, Q, and R-branches for different K values.

Results and Discussion

Theoretical Results

Table 1 lists the theoretical energies and zero point energies for several states of the $[Au,C,2H]^+$ system as calculated at the B3LYP/def2-TZVPPD level of theory. Selected geometric parameters are also provided. Several structures are possible and here we have considered the methylidene (carbene), $AuCH_2^+$; methylidyne (carbyne) hydride, $HAuCH^+$; and an adduct of the carbide with dihydrogen, $(H_2)AuC^+$. (The only other possibility, a dihydride carbide, $HAuHC^+$, was considered unlikely because gold cannot support the many covalent bonds needed to make it stable. Indeed, calculations attempting to find this species collapsed to $HAuCH^+$ structures.) The lowest energy species is the $AuCH_2^+$ ($^1A_1$) ground state, lying 1.3 eV below an excited triplet state, 2.5 – 3.2 eV below the $HAuCH^+$ structures, and 3.5 eV below the $(H_2)AuC^+$ structure. More

importantly, energies relative to the Au^+ (^1S) + C_2H_4O reactants are also provided and show that formation of $AuCH_2^+$ ($^1A_1$) + CH_2O is the only exothermic channel available (by 0.57 eV). This energy agrees reasonably well with experimental thermochemistry that specifies the reaction is exothermic by 0.32 ± 0.07 eV (= $D_0(CH_2O\text{-}CH_2) - D_0(Au^+\text{-}CH_2)$ = 3.376 ± 0.004[70] – 3.70 ± 0.07[38] eV). The modest difference of 0.25 ± 0.07 eV is similar to discrepancies noted between experiment and comparable levels of theory for similar reactions with 5d transition metal systems.[29-33, 35-38] Note also that the present calculations reproduce the experimental Au^+-CH_2 bond energy, 3.76 versus 3.70 ± 0.07 eV, and do a reasonable job predicting the singlet-triplet splitting of CH_2, 0.48 versus 0.390 ± 0.002[70] eV, Table 1. They also indicate that dissociation of $AuCH_2^+$ ($^1A_1$) to Au^+ + CH_2 ($^3B_1$) is similar in energy to the AuC^+ + H_2 asymptote (3.76 versus 4.00 eV), consistent with the observation by Metz and co-workers that photodissociation leads to both channels (with an onset of 3.86 eV).[57]

The geometry of the $AuCH_2^+$ ($^1A_1$) ground state is similar to those found in previous calculations.[38, 41, 59] We also located an excited triplet state that retains C_{2v} symmetry ($^3B_1$), but this has an imaginary frequency corresponding to an out-of-plane bend such that the true minimum is a $^3A'$ state having a ∠AuCHH dihedral angle of 155.1° and lying only 0.003 eV below the symmetric $^3B_1$ state. Symmetry dictates that the distorted $^3A'$ structure is one minimum of a double-well potential. The zero-point energy of the harmonic vibrational coordinate linking these two minima (the out-of-plane bend) is 0.022 eV, such that this structure can be considered as having time-averaged C_{2v} symmetry. Previous calculations also located a $^3A_1$ excited state lying 3.42 eV above the $^1A_1$ ground state, as well as singlet analogues of the two triplet states, $^1B_1$ and $^1A_2$, lying 1.44 and 4.63 above the ground state.[38] The latter were heavily spin-contaminated. As none of these excited states are likely to be important in the present study, they were not recalculated here.

Alternative structures for $[Au,C,2H]^+$ have not previously been considered theoretically. The present calculations find that the carbyne hydride structures also exhibited a singlet state as the lowest energy state (with the hydrogens in a cis configuration), with an excited triplet another 0.5 eV higher in energy. Here too, the planar $^3A''$ state has an imaginary out-of-plane torsion

leading to the distorted ^{3}A state having a ∠HAuCH dihedral angle of 64.4°. The distorted species lies 0.028 eV below the planar state before zero point energies are considered and by 0.011 eV after. We also found a trans configuration of the hydrogens in a singlet state lying 0.62 eV above the cis configuration. The dihydrogen adduct of AuC^+, $(H_2)AuC^+$ is high in energy because it nearly corresponds to the $AuC^+ + H_2$ product asymptote, only 0.43 eV higher in energy.

Table 2 lists the calculated vibrational frequencies for the lowest energy $[Au,C,2H]^+$ species in Table 1. Note that the anharmonic frequencies and the scaled harmonic frequencies of the ground state are nearly identical (differences ≤10 cm^{-1} for the four modes within the experimentally explored region). Although most of the frequencies and nature of vibrational modes are similar for the $AuCH_2^+$ carbene and $HAuCH^+$ carbyne hydride structures, several modes do change. The in-plane wag of CH_2 in the carbenes turns into the out-of-phase bend of $HAuCH^+$. The CH_2 scissor vibration in the carbenes becomes the in-phase in-plane bend of $HAuCH^+$. The symmetric and asymmetric CH stretches in the carbenes become the AuH and CH stretches of $HAuCH^+$.

Experimental Results

The IRMPD spectrum of $[Au,C,2H]^+$ is shown in Figure 1 and exhibits five resonances at 678, 745, 865 (with a shoulder at 812), 1006 (with a shoulder at ~1080), and 1343 cm^{-1}. Figure 1 also compares this spectrum to that calculated for the ground state $AuCH_2^+$ ($^1A_1$) species, with frequencies and intensities listed in Table 2. The strongest band is calculated to lie at 1004 cm^{-1}, and corresponds to the out-of-plane (oop) bend of the CH_2 group. The next most intense bands are predicted to lie at 632 (Au-C stretch) and 740 (in-plane CH_2 wag) cm^{-1}. These three bands correspond reasonably well with the observed spectrum both in position and relative intensities. A band at 1359 cm^{-1} (CH_2 scissors) is predicted to be relatively weak, consistent with the small peak observed at 1353 cm^{-1}. The only other predicted vibrations are the symmetric and asymmetric CH stretches lying at 3000 and 3118 cm^{-1}, respectively, outside the range of the present experiments. The weak band observed at 865 (and shoulder at 812) cm^{-1} does not appear to be associated with

a fundamental mode of $AuCH_2^+$ ($^1A_1$), nor with an overtone or combination band of this species. Furthermore, the spectrum for this species does not explain the shoulder observed at 1080 cm^{-1}, either. Thus, it seems clear that the main features of the experimental spectrum are explained by the $^1A_1$ ground state; however, the additional features at 865, 812, and 1080 cm^{-1} may indicate contributions from other sources.

Table 2 also lists frequencies calculated for the triplet excited state of $AuCH_2^+$ (both the planar and distorted forms). As shown in Figure 1, this spectrum does not match experiment at all (in particular, there is no experimental evidence for the strong resonances predicted at 358 and 1187 cm^{-1}), nor can it explain the resonances observed at 865 and 1080 cm^{-1}. Likewise, the singlet and triplet states of the carbyne hydride do not reproduce the experimental spectrum and there is no evidence for the strongest band predicted at 369 cm^{-1} ($HAuCH^+$, $^1A'$), Figure 1 and Table 2. Although this species does predict a band at 907 cm^{-1} (which could correspond to a shifted 865 cm^{-1} band), the failure to observe any intensity at 369 cm^{-1} and the high energy of formation of this species make it an unlikely contributor to the observed spectrum. Thus, we rule out the presence of $[Au,C,2H]^+$ species other than the $^1A_1$ CH_2^+ ground state.

As noted above, recent work has shown evidence of rotational band structure for the $[M,C,2H]^+$ and $[M,C,2D]^+$ species of M^+ = Ta^+, W^+, Os^+, Ir^+, and Pt^+.[47-48] Figure 2 shows the theoretical predictions including rotational band structure for the ground state $AuCH_2^+$ species at a rotational temperature of 77 K. (The exact temperature is unknown, but when a rotational temperature of 293 K is used, see Supporting Figure S3, the calculated bands are substantially broader than experiment.) Two versions are shown: one that excludes the nuclear spin statistical weights (3:1) associated with permutation of the two protons and one that includes this factor. We note that inclusion of this factor is particularly evident in the enhanced visibility of branches associated with odd K_a levels in b- and c-type transitions. In both cases, the highest frequency band shown (at 1359 cm^{-1}) shows closely spaced P and R branches characteristic of an a-type transition, consistent with the reasonably narrow peak observed at 1343 cm^{-1}. In contrast, the intense peak predicted at 1004 cm^{-1} is a c-type band with a broader rotational structure that

plausibly explains the "shoulder" observed at 1080 cm^{-1} (especially for the version including the nuclear spin statistics). The lowest resonance observed at 678 cm^{-1} appears to match the narrow P and R branches of the Au-C stretch (a-type) at 632 cm^{-1}, although clearly a blue-shift of 40 – 50 cm^{-1} would provide a better match. Notably, similar blue-shifts have also been required to match experiment for the predicted lowest energy bands of $DIrCD^+$ (50 cm^{-1}), $HOsCH^+$ (30 cm^{-1}), and $DOsCD^+$ (30 cm^{-1}).[47-48] The predicted band at 740 cm^{-1} (b-type in-plane bend) exhibits a broader rotational band structure that matches the frequency and relative intensity but not the width of the band observed at 745 cm^{-1}, although the version including the nuclear spin statistics may account for this better. Further, it is possible that the "shoulder" seen at 812 cm^{-1} could be attributed to the rotational structure of this band. The overall agreement between experiment and either simulation is quite reasonable, but the limited spectral resolution and the limited constraints in the simulations make it impossible to determine whether the species deviates from C_{2v} symmetry (obviating the need to include nuclear spin statistics), or not. Moreover, they still do not provide an explanation for the band at 865 cm^{-1}.

A more speculative interpretation of the data designed to explain this band notes that the experimental width of this band matches that predicted for the b-type in-plane bend at 740 cm^{-1}. If correct, then this predicted band would require a blue shift of about 90 cm^{-1} to match experiment, a much larger discrepancy than has been observed in previous related systems. Further, this assignment leaves the peak observed at 745 cm^{-1} unassigned. In this case, one possibility is that both the 632 and 740 cm^{-1} predicted bands need to be blue-shifted by about 90 cm^{-1}. Then, the P and R branches of the predicted a-type Au-C stretch band at 632 cm^{-1} are split (by 67 cm^{-1}) more than predicted and account for both the 678 and 745 cm^{-1} bands observed experimentally. Such a larger than simulated splitting is not unprecedented and has been observed for the a-type M-C stretches of $DIrCD^+$ (63 cm^{-1}) and $DOsCD^+$ (70 cm^{-1}),[47-48] although it was not found for the M-C stretch of the $PtCH_2^+$ ($^2A_1$) molecule. Overall, we do not find this speculative interpretation (which is shown in Supporting Figure S4) to be very satisfactory and therefore consider one other possibility.

Because the experimental spectrum for $[Au,C,2H]^+$ comes exclusively from the appearance of the AuC^+ product and no mass-selection is done prior to irradiation, it is possible that species other than $[Au,C,2H]^+$ also contribute. It seems unlikely that a contaminant is involved given the mass of the product. Therefore, we considered $AuC_2H_2^+$, $AuC_2H_4^+$, $AuCH_2O^+$, $AuC_2H_2O^+$, $AuC_2H_4O^+$, and $AuC_3H_6O^+$ species also formed in the reaction of Au^+ with ethylene oxide. All other species formed are too minor to contribute appreciably and they would have similar spectral features anyway because they are likely to be cC_2H_4O adducts of these species. These other product ions could plausibly dissociate to form AuC^+ by losses of CH_2, CH_4, H_2O, CH_2O, CH_4O (or $CH_2O + H_2$), and $C_2H_4O + H_2$, respectively, which are all stable molecules except for the CH_2 (making this channel unlikely). We attempted to verify this hypothesis experimentally by examining the frequency dependent depletion of these peaks in the mass spectrum. Because of the small intensities of all of these masses (see Figure S1), the results were not very definitive but *m/z* 255 ($AuC_3H_6O^+$) and most higher mass species showed depletion near 865 cm^{-1} (see Supporting Figure S5) and nowhere else. This frequency nearly coincides with the strongest band of free cC_2H_4O (observed at 877 cm^{-1} in absorption),[71] suggesting that *m/z* 255 (and the higher masses) are products containing intact c-C_2H_4O.

Consequently, we theoretically examined the IR spectra of all of the additional products mentioned above to see whether they could plausibly absorb near 865 cm^{-1}. As shown in Supporting Figure S6, the calculated spectra for $AuC_2H_2^+$, $AuC_2H_4^+$, and $AuCH_2O^+$ do not match the experimental spectrum nor do they have a band near 865 cm^{-1}. (The $AuC_2H_2^+$ spectrum does show bands at 735, 766, and 820 cm^{-1} that match the experimental 745 and 812 cm^{-1} peaks, but calculations indicate that loss of CH_2 from $AuC_2H_2^+$ to form AuC^+ requires over 8 eV, making this channel implausible. Further, this spectrum still does not reproduce the 865 cm^{-1} band.)

As shown in Figure 3, gold cation adducts of ethylene oxide, Au^+(c-C_2H_4O) (*m/z* 241), and dehydrogenated ethylene oxide, Au^+(c-C_2H_2O) (*m/z* 239), do exhibit peaks in the vicinity of 865 cm^{-1}. Furthermore, any additional peaks either lie under those for $AuCH_2^+$ ($^1A_1$) or have predicted intensities that are small enough that not observing them is a reasonable possibility. For

$Au^+(c\text{-}C_2H_4O)$, the most intense band predicted (over six times higher than any other mode) lies at 821 cm^{-1} (C-O stretch, 153 km/mol) and could plausibly reproduce the 865 cm^{-1} (or 812 cm^{-1} shoulder) with no additional perturbations to the bands of $AuCH_2^+$. For $Au^+(c\text{-}C_2H_2O)$, the two most intense bands lie at 655 cm^{-1} (CH out-of-plane bend, 62 km/mol) and 828 cm^{-1} (C-O stretch, 33 km/mol). Here, bands at 326 (15 km/mol) and 360 (16 km/mol) cm^{-1} of modest intensity might have been expected to be observed, but were not. Calculations indicate that loss of methanol from $Au^+(c\text{-}C_2H_4O)$ requires 4.57 eV (although this requires extensive rearrangement to form CH_3OH) or alternatively, it requires only 1.27 eV for the metallacycle to first cleave across the ring losing formaldehyde and yielding $AuCH_2^+$, which, if the system was sufficiently excited, retains enough energy to dehydrogenate. Likewise, loss of formaldehyde from $Au^+(c\text{-}C_2H_2O)$ requires only 2.52 eV. All these energetics are plausible for IRMPD processes. Nevertheless, these species did not exhibit depletions anywhere in the frequency range examined and the predicted bands (at 821 and 828 cm^{-1}) are somewhat lower in frequency than would match the experimental 865 cm^{-1} band with fidelity.

We also considered metallacyclobutene and metallacyclobutane structures for *m/z* 241 and *m/z* 239. The $c\text{-}AuCH_2OCH_2^+$ and $c\text{-}AuOC_2H_4^+$ metallacycles lie 0.10 and 0.86 eV, respectively, above the $Au^+(c\text{-}C_2H_4O)$ adduct. Likewise, the $c\text{-}AuCHOCH^+$ metallacycle lies 0.72 eV above the $Au^+(c\text{-}C_2H_2O)$ adduct. In contrast, optimization of a $c\text{-}AuOC_2H_2^+$ metallacycle leads to an $AuCHCHO^+$ structure having an ∠AuCCO dihedral angle of 92.6° and lying 1.55 eV *below* the $Au^+(c\text{-}C_2H_2O)$ adduct. In all four cases, their spectra contain intense features that are not found in the experimental spectrum, see Supporting Figure S7.

Finally, we examined the ethylene oxide adduct of $AuCH_2^+$ (*m/z* 255), the lowest mass species that did exhibit depletion near 865 cm^{-1}. Here, only the adduct form was examined theoretically because the metallacyclobutane forms are higher in energy (as noted immediately above) and are less likely to form once the Au^+-CH_2 bond is formed. The calculated spectrum for this species, $H_2CAu^+(c\text{-}C_2H_4O)$, is also shown in Figure 3. The spectrum is dominated by a very intense band at 867 cm^{-1} (CO stretch, 248 km/mol), more than five times as intense as any other

band (consistent with the intense band observed for free ethylene oxide[71]). Most of the other bands having modest intensities essentially match those of $AuCH_2^+$, so that they would be screened by fragmentation from that much more abundant species. Thus, the $H_2CAu^+(c\text{-}C_2H_4O)$ adduct seems the most likely candidate as the primary carrier of the band observed at 865 cm^{-1} (and possibly its 812 cm^{-1} shoulder). Presumably, this species dissociates primarily by loss of the intact ethylene oxide ligand (which according to theory requires 1.98 eV), but can absorb enough energy at 867 cm^{-1} that the remaining $AuCH_2^+$ fragment dissociates further by H_2 loss. It also seems possible that the 812 cm^{-1} band comes from the $Au^+(c\text{-}C_2H_4O)$ adduct (predicted resonance at 821 cm^{-1}) although this species did not show obvious depletion.

Nature of the Au^+-CH_2 Bond

As succinctly described by Irikura and Goddard,[41] transition metal bonds to CH_2 can be described by two limits: covalent and dative. In the covalent interaction, a CH_2 in its $^3B_1$ ground state interacts with a metal forming both a σ bond and a π bond. The σ bond involves the singly-occupied sp^2 (a_1) orbital on CH_2 and a s+dσ hybrid orbital on the metal. The π bond overlaps the p (b_1) orbital on CH_2 with a singly-occupied dπ orbital on the metal. In the dative interaction, the pair of electrons in the now doubly-occupied sp^2 (a_1) orbital of CH_2 in its $^1A_1$ excited state donates into an empty s+dσ hybrid orbital on the metal, while a pair of electrons in the metal dπ orbital donates into the now empty p (b_1) orbital of CH_2. Ultimately, both types of interactions lead to two electrons in both the σ and π bonds. The distinction between the two is thus a subtle one from the perspective of the orbital populations, although the two types of complexes do show distinctive reactivity in organometallic chemistry.[43, 72]

The valence orbitals of $AuCH_2^+$ ($^1A_1$) (excluding the $1a_1$ and $1b_2$ orbitals associated with the two CH bonds in CH_2) calculated at the B3LYP/def2-TZVPPD level are shown in Figure 4. The lowest energy orbital of these is the $2a_1$ orbital that clearly involves extensive 5dσ character along with contributions from the CH_2 (a_1) orbital. The $1b_1$ orbital is the π-backbonding orbital involving the 5dπ orbital and the CH_2 (b_1) orbital. The $2b_2$ orbital is the other 5dπ–like orbital, and

shows some antibonding character with the doubly occupied CH_2 (b_2) bonding orbital. The $3a_1$ and $1a_2$ orbitals are pure 5dδ orbitals. The highest occupied molecular orbital (HOMO), $4a_1$, is largely Au (6s) with some contributions from Au (5dσ) and CH_2 (a_1). Interestingly, an NBO analysis[73-74] of this system recognizes two Au-C bonds, a σ and a π, i.e., the $4a_1$ and $1b_1$ orbitals. All the other orbitals ($2a_1$, $2b_2$, $3a_1$, and $1a_2$) are described as lone pairs on the metal. The discrepancy between the orbital picture and the NBO analysis is a result of the different assumptions made regarding the construction of the MOs. In the NBO analysis, the lone pair $2a_1$ orbital is a s+dσ hybrid (86% 5dσ and 14% 6s). The $4a_1$ σ bond takes the other s+dσ hybrid (14% 5dσ and 86% 6s) and interacts this with the CH_2 (a_1) orbital such that it has 32% Au character and 68% C character (30% 2s and 70% 2p, i.e., sp^2). This breakdown is more closely aligned with donation of the electrons from CH_2 to an empty orbital on Au, i.e., the dative bonding picture. For the $1b_1$ π bond, the character switches to 87% Au (5dπ) and 13% C (2pπ). Here, the breakdown indicates mostly donation of a pair of electrons on Au into the empty p orbital on CH_2 ($^1A_1$), again dative bonding. Indeed, this analysis is comparable to that of Irikura and Goddard,[41] who found that the metal character in the Au^+-CH_2 σ and π bonds was about 25% and 95%, respectively.

When viewed independently, it seems clear that the bonding in $AuCH_2^+$ ($^1A_1$) is near the dative limit, resulting from the interaction of ground state Au^+ (^1S, $5d^{10}$) with excited state CH_2 ($^1A_1$). What makes this conclusion less clear is comparison to other 5d metals, e.g., $PtCH_2^+$ ($^2A_1$), which also exhibits the classic C_{2v} symmetry.[46-47] Calculations on this molecule at the same level of theory show that the orbitals are nearly identical to those shown in Figure 4. The only difference is that the $4a_1$ MO is only singly occupied rather than doubly occupied as in $AuCH_2^+$ ($^1A_1$). However, $PtCH_2^+$ has a metal-carbon bond strength that is considerably higher than that for $AuCH_2^+$: 4.80 ± 0.03 versus 3.70 ± 0.07 eV.[29, 34, 38] Thus, removing an electron from the MO characterized above as the σ bond *strengthens* the interaction. This observation suggests that in $PtCH_2^+$ (and perhaps $AuCH_2^+$), the $2a_1$ MO should also be considered as bonding, in contrast to the NBO analysis. Nevertheless, the NBO analysis of $PtCH_2^+$ ($^2A_1$) provides results similar to those for $AuCH_2^+$, with a doubly occupied π bond ($1b_1$) that is still largely metal based (77% Pt 5dπ and

23% C 2p versus 87 and 13% for $AuCH_2^+$) and the singly occupied σ bond ($4a_1$) that is more heavily given by the CH_2: 34% on Pt and 66% on C (versus 32% and 68% for $AuCH_2^+$). Also the s+dσ hybridization is distinct with 77% 6s and 22% 5dσ (versus 86% and 14% for $AuCH_2^+$). Again this agrees reasonably well with the analysis of Irikura and Goddard,[41] who characterized the σ bond in $PtCH_2^+$ as having about 40% Pt character (up from 25% for Au) and the π bond as having about 70% Pt character (down from about 95% for Au).

Overall, it can be realized that neither the pure covalent nor the pure dative bonding picture is correct for any single molecule, but rather that they represent extremes in the correct representation of how metals and carbon share electrons. In the case of $AuCH_2^+$, the picture of dative bonding seems most accurate, but the distinction from its nearest neighbor, $PtCH_2^+$, is a subtle one that is not completely captured by referring to the molecular orbitals nor by more sophisticated means of breaking down the bonding.

Conclusion

IRMPD action spectra of $[Au,C,2H]^+$ formed by reaction of gold cations with ethylene oxide were measured over the 300 – 1850 cm^{-1} spectral range. This spectrum is obtained by monitoring formation of AuC^+, whose experimental appearance spectrum agrees well with that calculated for the ground state $AuCH_2^+$ ($^1A_1$) carbene structure better than any other excited states or alternative structures, such as $HAuCH^+$ or $(H_2)AuC^+$. Indeed, no evidence for higher spin states or for these alternative structures was found in the experimental spectrum. The comparison between the experimental and theoretical spectra is assisted by including the complete rotational band structure in the calculated spectra. As in a previous studies,[47-48] rotational contours can have appreciable effects on the appearance of IRMPD spectral bands, thereby explaining the broadness of several bands (including the shoulder at 1080 cm^{-1}). Despite the general agreement, there is one additional band found at 865 cm^{-1} in the AuC^+ appearance spectrum that is not reproduced by $AuCH_2^+$ ($^1A_1$). Experimental evidence suggests that the ethylene oxide adduct of $AuCH_2^+$ is the origin of this band. Indeed, this species has a very intense absorption predicted at 867 cm^{-1},

matching the extra band well. Contributions from the ethylene oxide adduct of Au^+ are also plausible at 812 cm^{-1}. Theoretical analysis of the bonding in $AuCH_2^+$ ($^1A_1$) matches that in the literature, which concludes that the bonding is largely dative; however, the distinction between this picture and a more covalent one is subtle.

Associated Content

Supporting Information

The Supporting Information is available free of charge on the ACS Publications website at DOI: 10.1021/acs.jpca.xxxxx.

Table S1 provides information needed to calculate the rotational contours: dipole derivatives, principle axes, and moments of inertia of $AuCH_2^+$ ($^1A_1$). Figure S1 shows representative mass spectra of the ionic species formed from gold laser ablation in a flow of ethylene oxide mixed with He with and without laser irradiation at 1010 cm^{-1}. Figure S2 illustrates the geometric orientation of the Cartesian principle axes used in the calculation of dipole derivatives and moments of inertia of the ground states of $AuCH_2^+$. Figure S3 shows the spectra for $AuCH_2^+$ ($^1A_1$) including rotational band structure at 293 K both with and without including nuclear spin statistics. Figure S4 shows the spectrum for $AuCH_2^+$ ($^1A_1$) including the rotational band contours at 77 K and the two lowest frequency bands blue-shifted by 90 cm^{-1}. Figure S5 shows representative mass spectra of the ionic species formed from gold laser ablation in a flow of ethylene oxide mixed with He with and without laser irradiation at 836 cm^{-1}. Figures S6 and S7 show comparisons of the calculated spectra for alternative precursors with the experimental spectrum.

Author Information

Corresponding Author

*E-mail: armentrout@chem.utah.edu

ORCID

P. B. Armentrout: 0000-0003-2953-6039

J. M. Bakker: 0000-0002-1394-7661

Notes

The authors declare no competing financial interest.

Acknowledgements

Profs. Michael Morse (who first pointed out the need to include the nuclear spin statistics) and Leo Meerts graciously lended their expertise to the generation of the rotational contour bands. We gratefully acknowledge the Nederlandse Organisatie voor Wetenschappelijk Onderzoek (NWO) for support of the FELIX Laboratory and support for this project was provided by the National Science Foundation, Grant Nos. CHE-1664618 and OISE-1357887. Finally, the Center for High Performance Computing (CHPC) at the University of Utah is acknowledged for their generous allocation of computing time.

References

1. Bharadwaj, S. S.; Schmidt, L. D. Catalytic Partial Oxidation of Natural-Gas to Syngas. *Fuel Process. Technol.* **1995,** *42*, 109-127.
2. Lee, Y. J.; Hong, S. I.; Moon, D. J. Studies on the Steam and CO_2 Reforming of Methane for GTL-FPSO Applications. *Catal. Today* **2011,** *174*, 31−36.
3. Schwarz, H. Chemistry with Methane: Concepts Rather than Recipes. *Angew. Chem. Int. Ed.* **2011,** *50*, 10096-10115.
4. Roithová, J.; Schröder, D. Selective Activation of Alkanes by Gas-Phase Metal Ions. *Chem. Rev.* **2010,** *110*, 1170–1211.
5. Irikura, K. K.; Beauchamp, J. L. Electronic Structure Considerations for Methane Activation by Third-row Transition-metal Ions. *J. Phys. Chem.* **1991,** *95*, 8344-8351.
6. Shayesteh, A.; Lavrov, V. V.; Koyanagi, G. K.; Bohme, D. K. Reactions of Atomic Cations with Methane: Gas Phase Room-Temperature Kinetics and Periodicities in Reactivity. *J. Phys. Chem. A* **2009,** *113*, 5602–5611.
7. Allison, J. The Gas-Phase Chemistry of Transition-Metal Ions with Organic Molecules. *Prog. Inorg. Chem.* **1986,** *34*, 627-676.
8. Squires, R. R. Gas-phase Transition-metal Negative Ion Chemistry. *Chem. Rev.* **1987,** *87*, 623-646.
9. Aristov, N.; Armentrout, P. B. Methane Activation by V^+: Electronic and Translational Energy Dependence. *J. Phys. Chem.* **1987,** *91*, 6178-6188.

10. Sunderlin, L. S.; Armentrout, P. B. Methane Activation by Ti^+: Electronic and Translational Energy Dependence. *J. Phys. Chem.* **1988,** *92*, 1209-1219.
11. Schultz, R. H.; Elkind, J. L.; Armentrout, P. B. Electronic Effects in C-H and C-C Bond Activation: State-specific Reactions of $Fe^+(^6D, ^4F)$ with Methane, Ethane and Propane. *J. Am. Chem. Soc.* **1988,** *110*, 411-423.
12. Georgiadis, R.; Armentrout, P. B. Translational and Electronic Energy Dependence of Chromium Ion Reactions with Methane. *J. Phys. Chem.* **1988,** *92*, 7067-7074.
13. Sunderlin, L. S.; Armentrout, P. B. Periodic Trends in Chemical Reactivity: Reactions of Sc^+, Y^+, La^+, and Lu^+ with Methane and Ethane. *J. Am. Chem. Soc.* **1989,** *111*, 3845-3855.
14. Russell, D. H., *Gas Phase Inorganic Chemistry*. Plenum: New York, 1989.
15. Eller, K.; Schwarz, H. Organometallic Chemistry in the Gas Phase. *Chem. Rev.* **1991,** *91*, 1121-1177.
16. Chen, Y.-M.; Armentrout, P. B. Activation of Methane by Gas-Phase Rh^+. *J. Phys. Chem.* **1995,** *99*, 10775-10779.
17. Armentrout, P. B.; Kickel, B. L., Gas-Phase Thermochemistry of Transition Metal Ligand Systems: Reassessment of Values and Periodic Trends. In *Organometallic Ion Chemistry*, Freiser, B. S., Ed. Kluwer: Dordrecht, 1996; pp 1-45.
18. Haynes, C. L.; Chen, Y.-M.; Armentrout, P. B. The Potential Energy Surface for Activation of Methane by Co^+: An Experimental Study. *J. Phys. Chem.* **1995,** *99*, 9110-9117.
19. Haynes, C. L.; Chen, Y.-M.; Armentrout, P. B. The Reaction of $FeCH_2^+ + D_2$: Probing the $[FeCH_4]^+$ Potential Energy Surface. *J. Phys. Chem.* **1996,** *100*, 111-119.
20. Chen, Y.-M.; Sievers, M. R.; Armentrout, P. B. Activation of CH_4, C_2H_6, C_3H_8, and c-C_3H_6 by Gas-phase Pd^+ and the Thermochemistry of Pd-ligand Complexes. *Int. J. Mass Spectrom. Ion Processes* **1997,** *167/168*, 195-212.
21. Armentrout, P. B., Gas Phase Organometallic Chemistry. In *Topics in Organometallic Chemistry*, Brown, J. M.; Hofmann, P., Eds. Springer-Verlag: Berlin, 1999; Vol. 4, pp 1-45.
22. Sievers, M. R.; Chen, Y.-M.; Haynes, C. L.; Armentrout, P. B. Activation of CH_4, C_2H_6, and C_3H_8 by Gas-Phase Nb^+ and the Thermochemistry of Nb-ligand complexes. *Int. J. Mass Spectrom.* **2000,** *195/196*, 149-170.
23. Armentrout, P. B.; Sievers, M. R. Activation of CH_4 by Gas-phase Zr^+ and the Thermochemistry of Zr ligand Complexes. *J. Phys. Chem. A* **2003,** *107*, 4396-4406.
24. Liu, F.; Zhang, X.-G.; Armentrout, P. B. Activation of CH_4 by Gas-phase Ni^+ and the Thermochemistry of Ni Ligand Complexes. *Phys. Chem. Chem. Phys.* **2005,** *7*, 1054-1064.
25. Armentrout, P. B. Activation of CH_4 by Gas-phase Mo^+ and the Thermochemistry of Mo-ligand Complexes. *J. Phys. Chem. A* **2006,** *110*, 8327-8338.
26. Irikura, K. K.; Beauchamp, J. L. Osmium Tetroxide and Its Fragment Ions in the Gas Phase: Reactivity with Hydrocarbons and Small Molecules. *J. Am. Chem. Soc.* **1989,** *111*, 75-85.
27. Buckner, S. W.; MacMahon, T. J.; Byrd, G. D.; Freiser, B. S. Gas-Phase Reactions of Nb^+ and Ta^+ with Alkanes and Alkenes. C-H Bond Activation and Ligand-Coupling Mechanisms. *Inorg. Chem.* **1989,** *28*, 3511-3518.
28. Irikura, K. K.; Beauchamp, J. L. Methane Oligomerization in the Gas Phase by Third-Row Transition-Metal Ions. *J. Am. Chem. Soc.* **1991,** *113*, 2769-2770.
29. Zhang, X.-G.; Liyanage, R.; Armentrout, P. B. The Potential Energy Surface for Activation of Methane by Pt^+: A Detailed Guided-Ion Beam Study. *J. Am. Chem. Soc.* **2001,** *123*, 5563-5575.

30. Armentrout, P. B.; Shin, S.; Liyanage, R. Guided-Ion Beam and Theoretical Study of the Potential Energy Surface for Activation of Methane by W^+ *J. Phys. Chem. A* **2006,** *110*, 1242-1260.
31. Li, F.-X.; Zhang, X.-G.; Armentrout, P. B. The Most Reactive Third-row Transition Metal: Guided Ion Beam and Theoretical Studies of the Activation of Methane by Ir^+. *Int. J. Mass Spectrom.* **2006,** *255/256*, 279-300.
32. Parke, L. G.; Hinton, C. S.; Armentrout, P. B. Experimental and Theoretical Studies of the Activation of Methane by Ta^+ and the Bond Energies of Ta^+-CH_x (x = 1 - 3). *J. Phys. Chem. C* **2007,** *111*, 17773-17787.
33. Armentrout, P. B.; Parke, L.; Hinton, C.; Citir, M. Activation of Methane by Os^+: Guided Ion Beam and Theoretical Studies. *ChemPlusChem* **2013,** *78*, 1157-1173.
34. Armentrout, P. B. Methane Activation by 5d Transition Metals: Energetics, Mechanisms, and Periodic Trends. *Chem.: Eur. J.* **2017,** *23*, 10-18.
35. Armentrout, M. M.; Li, F.-X.; Armentrout, P. B. Is Spin Conserved in Heavy Metal Systems? Experimental and Theoretical Studies of the Reaction of Re^+ with Methane. *J. Phys. Chem. A* **2004,** *108*, 9660-9672.
36. Parke, L. G.; Hinton, C. S.; Armentrout, P. B. Why is Hafnium So Unreactive? Experimental and Theoretical Studies of the Reaction of Hf^+ with Methane. *Int. J. Mass Spectrom.* **2006,** *254*, 168-182.
37. Parke, L. G.; Hinton, C. S.; Armentrout, P. B. Energetics and Mechanisms of C-H Bond Activation by a Doubly-charged Metal Ion: Guided Ion Beam and Theoretical Studies of Ta^{2+} + CH_4. *J. Phys. Chem. A* **2008,** *112*, 10469–10480.
38. Li, F.-X.; Armentrout, P. B. Activation of Methane by Gold Cations: Guided Ion Beam and Theoretical Studies. *J. Chem. Phys.* **2006,** *125*, 133114
39. Lang, S. M.; Bernhardt, T. M.; Barnett, R. N.; Landman, U. Methane Activation and Catalytic Ethylene Formation on Free Au_2^+. *Angew. Chem. Int. Ed.* **2010,** *49*, 980-983.
40. Shuman, N. S.; Ard, S. G.; Sweeny, B. C.; Pan, H.; Viggiano, A. A.; Keyes, N. R.; Guo, H.; Owen, C. J.; Armentrout, P. B. Au_2^+ Cannot Catalyze Conversion of Methane to Ethene at Low Temperature. *Catal. Sci. Tech.* **2019,** *9*, 2767-2780.
41. Irikura, K. K.; Goddard III, W. A. Energetics of Third-Row Transition Metal Methylidene Ions MCH_2^+ (M = La, Hf, Ta, W, Re, Os, Ir, Pt, Au). *J. Am. Chem. Soc.* **1994,** *116*, 8733-8740.
42. Simon, A.; Lemaire, J.; Boissel, P.; Maître, P. Competition Between Agostic WCH_2^+ and $HWCH^+$: A Joint Experimental and Theoretical Study *J. Chem. Phys.* **2001,** *115*, 2510-2518.
43. Schrock, R. R. Alkylidene Complexes of Niobium and Tantalum. *Acc. Chem. Res.* **1979,** *12*, 98-104.
44. Goddard, R. J.; Hoffmann, R.; Jemmis, E. D. Unusual Metal-Carbon-Hydrogen Angles, Carbon-Hydrogen Bond Activation, and -Hydrogen Abstraction in Transition-Metal Carbene Complexes. *J. Am. Chem. Soc.* **1980,** *102*, 7667-7676.
45. Brookhart, M.; Green, M. L. H. Carbon-Hydrogen–Transition Metal Bonds. *J. Organomet. Chem.* **1983,** *250*, 395–408.
46. Lapoutre, V. J. F.; Redlich, B.; van der Meer, A. F. G.; Oomens, J.; Bakker, J. M.; Sweeney, A.; Mookherjee, A.; Armentrout, P. B. Structures of the Dehydrogenation Products of Methane Activation by 5d Transition Metal Cations. *J. Phys Chem. A* **2013,** *117*, 4115-4126.
47. Owen, C. J.; Boles, G. C.; Chernyy, V.; Bakker, J. M.; Armentrout, P. B. Structures of the Dehydrogenation Products of Methane Activation by 5d Transition Metal Cations Revisited: Deuterium Labeling and Rotational Contours. *J. Chem. Phys.* **2018,** *148*, 044307.

48. Armentrout, P. B.; Kuijpers, S.; Lushchikova, O.; Hightower, R. L.; Boles, G. C.; Bakker, J. M. Spectroscopic Identification of the Carbyne Hydride Structure of the Dehydrogenation Product of Methane Activation by Osmium Cations. *J. Am. Soc. Mass Spectrom.* **2018,** *29*, 1781-1791.
49. Brümmer, M.; Kaposta, C.; Santambrogio, G.; Asmis, K. R. Formation and Photodepletion of Cluster Ion-Messenger Atom Complexes in a Cold Ion Trap: Infrared Spectroscopy of VO^+, VO_2^+, and VO_3. *J. Chem. Phys.* **2003,** *119*, 12700–12703.
50. Lang, S. M.; Bernhardt, T. M.; Chernyy, V.; Bakker, J. M.; Barnett, R. N.; Landman, U. Selective C−H Bond Cleavage in Methane by Small Gold Clusters. *Angew. Chem. Int. Ed.* **2017,** *56*, 13406-13410.
51. Wheeler, O. W.; Salem, M.; Gao, A.; Bakker, J. M.; Armentrout, P. B. Activation of C-H bonds in $Pt^+ + xCH_4$ Reactions, Where x = 1 – 4: Identification of the Platinum Dimethyl Cation. *J. Phys. Chem. A* **2016,** *120*, 6216–6227.
52. Letokhov, V. S.; Ryabov, E. A.; Tumanov, O. A. Luminiscence of a Molecular Gas under the Action of CO_2 Laser Pulses. *Sov. Phys. JETP* **1973,** *36*, 1069−1073.
53. Campbell, J. D.; Hancock, G.; Halpern, J. B.; Welge, K. H. Off Resonant Dissociation of NH_3 to Ground State Fragments by Pulsed CO_2 Laser Radiation. *Chem. Phys. Lett.* **1976,** *44*, 404−410.
54. Bakker, J. M.; Lapoutre, V. J. F.; Redlich, B.; Oomens, J.; Sartakov, B. G.; Fielicke, A.; von Helden, G.; Meijer, G.; van der Meer, A. F. G. Intensity-resolved IR Multiple Photon Ionization and Fragmentation of C_{60}. *J. Chem. Phys.* **2010,** *132*, 074305.
55. Lehmann, K. K.; Scoles, G.; Pate, B. H. Intramolecular Dynamics from Eigenstate-Resolved Infrared-Spectra. *Annu. Rev. Phys. Chem.* **1994,** *45*, 241−274.
56. Beil, A.; Luckhaus, D.; Quack, M.; Stohner, J. Intramolecular Vibrational Redistribution and Unimolecular Reaction: Concepts and New Results on the Femtosecond Dynamics and Statistics in CHBrClF. *Ber. Bunsen Phys. Chem.* **1997,** *101*, 311−328.
57. Aguirre, F.; Husband, J.; Thompson, C. J.; Metz, R. B. Gas-phase Photodissociation of $AuCH_2^+$: The Dissociation Threshold of Jet-cooled and Rotationally Thermalized Ions. *Chem. Phys. Lett.* **2000,** *318*, 466-470.
58. Chowdhury, A. K.; Wilkins, C. L. Reactions of Atomic Gold Ions with Aliphatic and Aromatic Hydrocarbons and Alkyl Halides. *J. Am. Chem. Soc.* **1987,** *109*, 5336-5343.
59. Heinemann, C.; Hertwig, R. H.; Wesendrup, R.; Koch, W.; Schwarz, H. Relativistic Effects on Bonding in Cationic Transition-Metal-Carbene Complexes: A Density-Functional Study. *J. Am. Chem. Soc.* **1995,** *117*, 495-500.
60. Hrusak, J. Relativistic Effects in the Metal-carbon Bond. A Comparative Ab Initio and DFT Study of $M{=}CH_2^+$ and $M\text{-}CH_3^+$ (M=Cu, Ag and Au). *S. Afr. J. Chem.* **1997,** *50*, 93-101.
61. Oomens, J.; Sartakov, B. G.; Meijer, G.; von Helden, G. Gas-phase Infrared Multiple Photon Dissociation Spectroscopy of Mass-selected Molecular Ions. *Int. J. Mass Spectrom.* **2006,** *254*, 1-19.
62. Dietz, T. G.; Duncan, M. A.; Powers, D. E.; Smalley, R. E. Laser Production of Supersonic Metal Cluster Beams. *J. Chem. Phys.* **1981,** *74*, 6511-6512.
63. Haertelt, M.; Lapoutre, V. J. F.; Bakker, J. M.; Redlich, B.; Fielicke, A.; Meijer, G. Structure Determination of Anionic Metal Clusters via Infrared Resonance Enhanced Multiple Photon Electron Detachment Spectroscopy. *J. Phys. Chem. Lett.* **2011,** *2*, 1720-1724.

64. Frisch, M. J.; Trucks, G. W.; Schlegel, H. B.; Scuseria, G. E.; Robb, M. A.; Cheeseman, J. R.; Scalmani, G.; Barone, V.; Petersson, G. A.; Nakatsuji, H., et al. *Gaussian 16, Revision A.03*, Gaussian, Inc.: Wallingford CT, 2016.
65. Becke, A. D. Density-functional Thermochemistry. III. The Role of Exact Exchange. *J. Chem. Phys.* **1993,** *98*, 5648-5652.
66. Lee, C.; Yang, W.; Parr, R. G. Development of the Colle-Salvetti Correlation-Energy Formula into a Functional of the Electron Density. *Phys. Rev. B* **1988,** *37*, 785-789.
67. Andrae, D.; Haeussermann, U.; Dolg, M.; Stoll, H.; Preuss, H. Energy-adjusted Ab Initio Pseudopotentials for the Second and Third Row Transition Elements. *Theor. Chim. Acta* **1990,** *77*, 123-141.
68. Kesharwani, M. K.; Brauer, B.; Martin, J. M. L. Frequency and Zero-Point Vibrational Energy Scale Factors for Double-Hybrid Density Functionals (and Other Selected Methods): Can Anharmonic Force Fields Be Avoided? *J. Phys. Chem. A* **2014,** *119*, 1701-1714.
69. Meerts, W. L.; Schmitt, M. Application of Genetic Algorithms in Automated Assignments of High-Resolution Spectra. *Int. Rev. Phys. Chem.* **2006,** *25*, 353-406.
70. Ruscic, B.; Bross, D. H. Active Thermochemical Tables (ATcT) values based on ver. 1.122e of the Thermochemical Network. Argonne National Laboratory (2019); available at ATcT.anl.gov
71. Nakanaga, T. Infrared Band Intensities of Ethylene Oxide. *J. Chem. Phys.* **1981,** *74*, 5384-5392.
72. Fischer, E. O., On the Way to Carbene and Carbyne Complexes. In *Adv. Organomet. Chem.*, Stone, F. G. A.; West, R., Eds. Academic Press: 1976; Vol. 14, pp 1-32.
73. Glendening, E. D.; Reed, A. E.; Carpenter, J. E.; Weinhold., F. *NBO Version 3.1*.
74. Foster, J. P.; Weinhold, F. Natural Hybrid Orbitals. *J. Am. Chem. Soc.* **1980,** *102*, 7211-7218.

Table 1. Calculated Electronic Energy, Vibrational Zero-Point Energy (ZPE), Relative Energy (E_{rel}), Bond Distances (Å), and Bond Angles (°) of $[Au,C,2H]^+$ and Related Species.[a]

Species	State	Energy (E_h)	ZPE (E_h)[b]	E_{rel} (eV)	r(AuC) (Å)	r(CH) (Å)	r(AuH) (Å)	∠AuCH (°)	∠HAuC (°)
$Au^+ + C_2H_4O$	$^1S + {}^1A_1$	-289.271620	0.056644	(0.57)[c]					
$AuCH_2^+$	$^1A_1$	-174.729053	0.022757	0.00	1.896	1.090 (2)		121.8(2)	
	$^3A'$	-174.677372	0.020547	1.35	1.996	1.085 (2)		113.0(2)	
	$^3B_1$	-174.677256	0.019785(i)	1.33	1.990	1.083 (2)		112.0(2)	
$HAuCH^+$	$^1A'$ (cis)	-174.630529	0.017482	2.54	1.856	1.106	1.581	125.1	118.0
	$^1A'$ (trans)	-174.606447	0.016340	3.16	1.998	1.129	1.541	96.2	85.4
	^3A	-174.613884	0.016682	2.97	1.918	1.093	1.558	135.4	89.8
	$^3A''$	-174.612847	0.016061(i)	2.98	1.924	1.092	1.557	140.9	89.9
$(H_2)AuC^+$	$^1A_1$	-174.589946	0.014843	3.57	1.835	0.771[d]	2.107 (2)		169.5
$Au^+ + CH_2$	$^1S + {}^3B_1$	-174.585008	0.016984	3.76		1.078		135.1	
	$^1S + {}^1A_1$	-174.566778	0.016247	4.24		1.109		101.9	
$AuC^+ + H_2$	$^1\Sigma + {}^1\Sigma$	-174.571162	0.011716	4.00	1.798	0.743[d]			

[a] All values obtained at the B3LYP/def2-TZVPPD level. [b] Frequencies were scaled by 0.9885.[68] Systems having an imaginary frequency are denoted by (i). [c] Energy of $Au^+ + C_2H_4O$ relative to $AuCH_2^+(^1A_1) + CH_2O$ where the calculated energy of CH_2O is -114.555950 E_h and its ZPE is 0.026214 E_h. [d] r(HH).

Table 2. Calculated Vibrational Frequencies (cm^{-1}) and IR Intensities (km/mol) of $[Au,C,2H]^+$ [a]

mode	Exp.	$AuCH_2^+$ ($^1A_1$)	Anharm.	$AuCH_2^+$ ($^3A'$)	$AuCH_2^+$ ($^3B_1$)	$HAuCH^+$ ($^1A'$)	$HAuCH^+$ (^3A)
Au-C stretch	678	632 (37)	635	522 (19)	527 (19)	*672 (61)*	*610 (27)*
CH_2 (*HAuCH*) in-plane wag	745 865[b]	740 (21)	743	646 (5)	644 (6)	*369 (95)*	*400 (10)*
CH_2 (*HAuCH*) oop bend	1006 (1080)[c]	1004 (66)	1014	358 (41)	i262 (33)	*617 (35)*	*307 (15)*
CH_2 scissors (*AuCH bend*)	1343	1359 (11)	1357	1187 (59)	1188 (78)	*907 (33)*	*791 (21)*
CH_2 sym. (*AuH*) stretch		3000 (20)	2956	2997 (54)	3005 (56)	*2076 (29)*	*2091 (103)*
CH_2 asym. (*CH*) stretch		3118 (43)	3055	3186 (59)	3202 (68)	*2929 (20)*	*3024 (96)*

[a] All theoretical harmonic vibrational frequencies have been scaled by 0.975. Anharmonic frequencies for the ground state are unscaled. Intensities in km/mol in parentheses. Values for carbyne hydride structures are in italics. [b] Assigned to $AuCH_2^+$(c-C_2H_4O), see text. [c] Assigned to rotational structure of the 1006 cm^{-1} band, see text.

Figure Captions

Figure 1. IRMPD spectrum for formation of $[Au,C]^+$ (black) and DFT calculated spectra for the singlet and triplet carbene $AuCH_2^+$ (top and middle traces, red) and singlet carbyne hydride $HAuCH^+$ (bottom trace, blue).

Figure 2. IRMPD spectra for formation of $[Au,C]^+$ (black) and the DFT calculated spectra including rotational band structure at 77 K excluding (top panel) and including (bottom panel) nuclear spin statistics for the singlet carbene $AuCH_2^+$ (red).

Figure 3. IRMPD spectra for formation of $[Au,C]^+$ (black) and the DFT calculated spectra of ethylene oxide adducts of gold carbene and gold atom cations, $H_2CAu^+(c\text{-}C_2H_4O)$ (green) and $Au^+(cC_2H_4O)$ (red), and gold cation with dehydrogenated ethylene oxide, $Au^+(cC_2H_2O)$ (blue).

Figure 4. Valence molecular orbitals for $AuCH_2^+$ ($^1A_1$) calculated at the B3LYP/def2-TZVPPD level of theory. The $1a_1$ and $1b_2$ orbitals corresponding to the CH_2 bonding orbitals are not included.

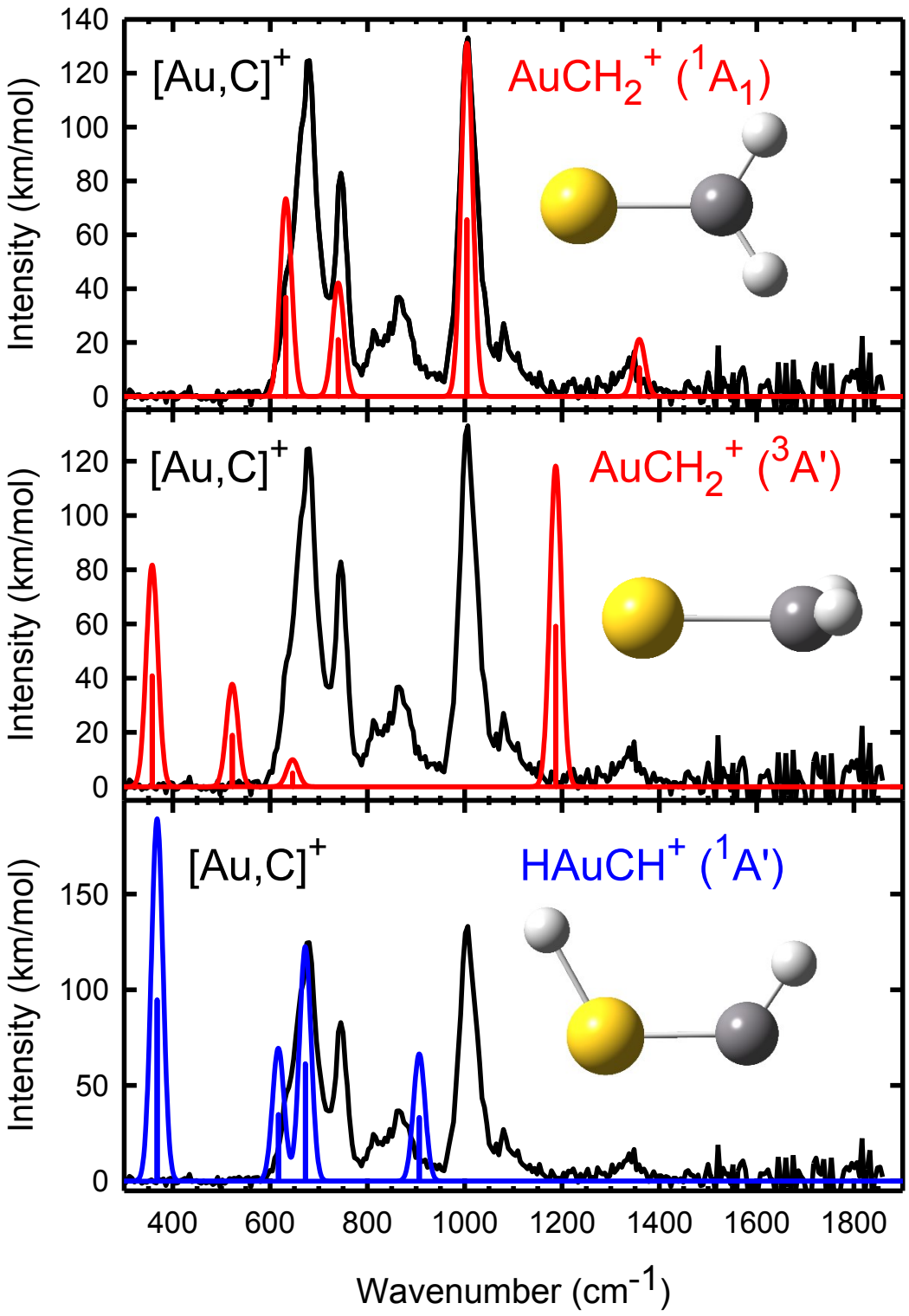
[Au,C]+
AuCH2+ (1A1)
[Au,C]+
AuCH2+ (3A')
[Au,C]+
HAuCH+ (1A')
Intensity (km/mol)
Wavenumber (cm-1)

Figure 1

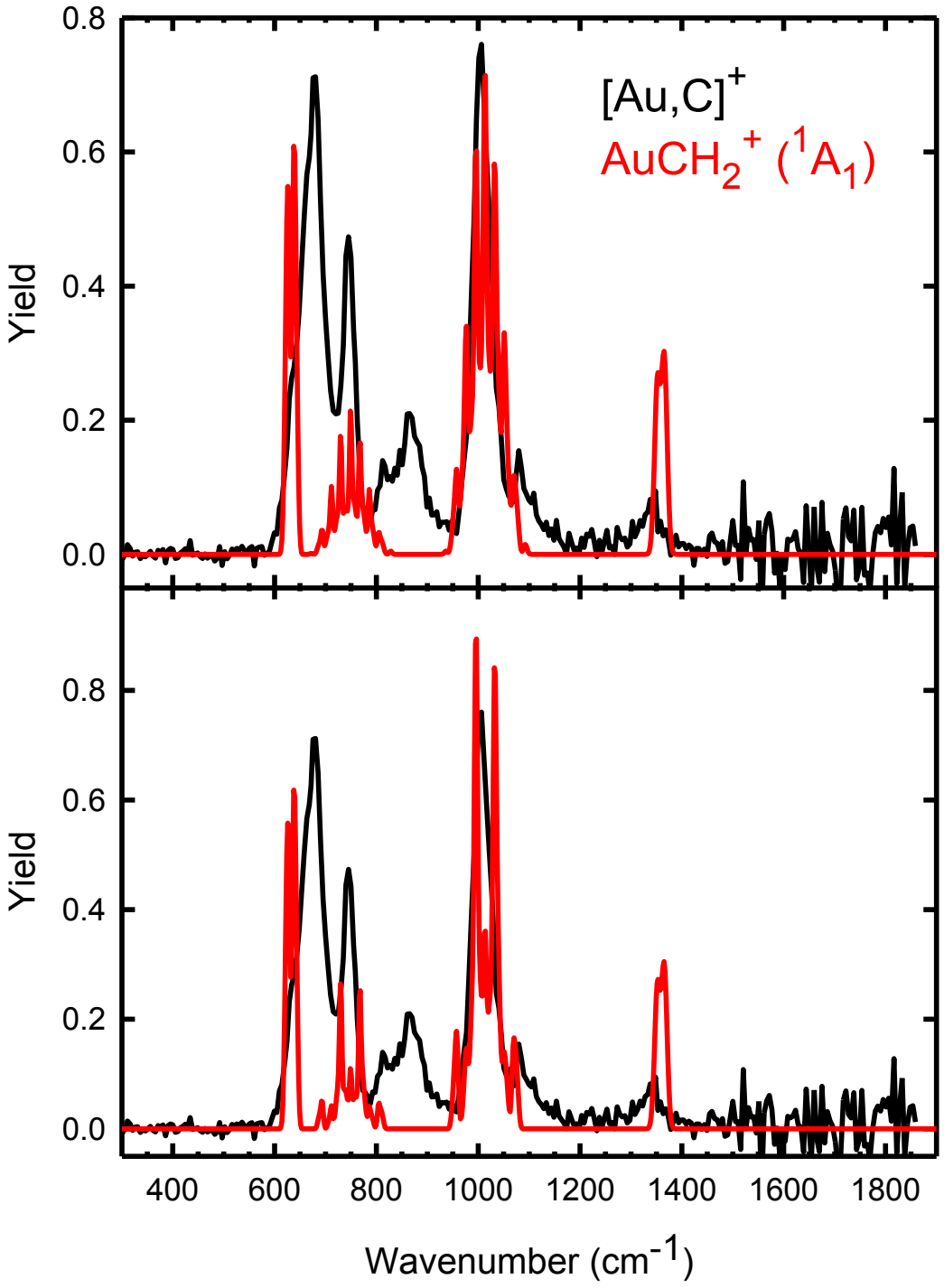
[Au,C]+
AuCH2+ (1A1)
Yield
Yield
0.0
0.2
0.4
0.6
0.8
400
600
800
1000
1200
1400
1600
1800
Wavenumber (cm-1)

Figure 2

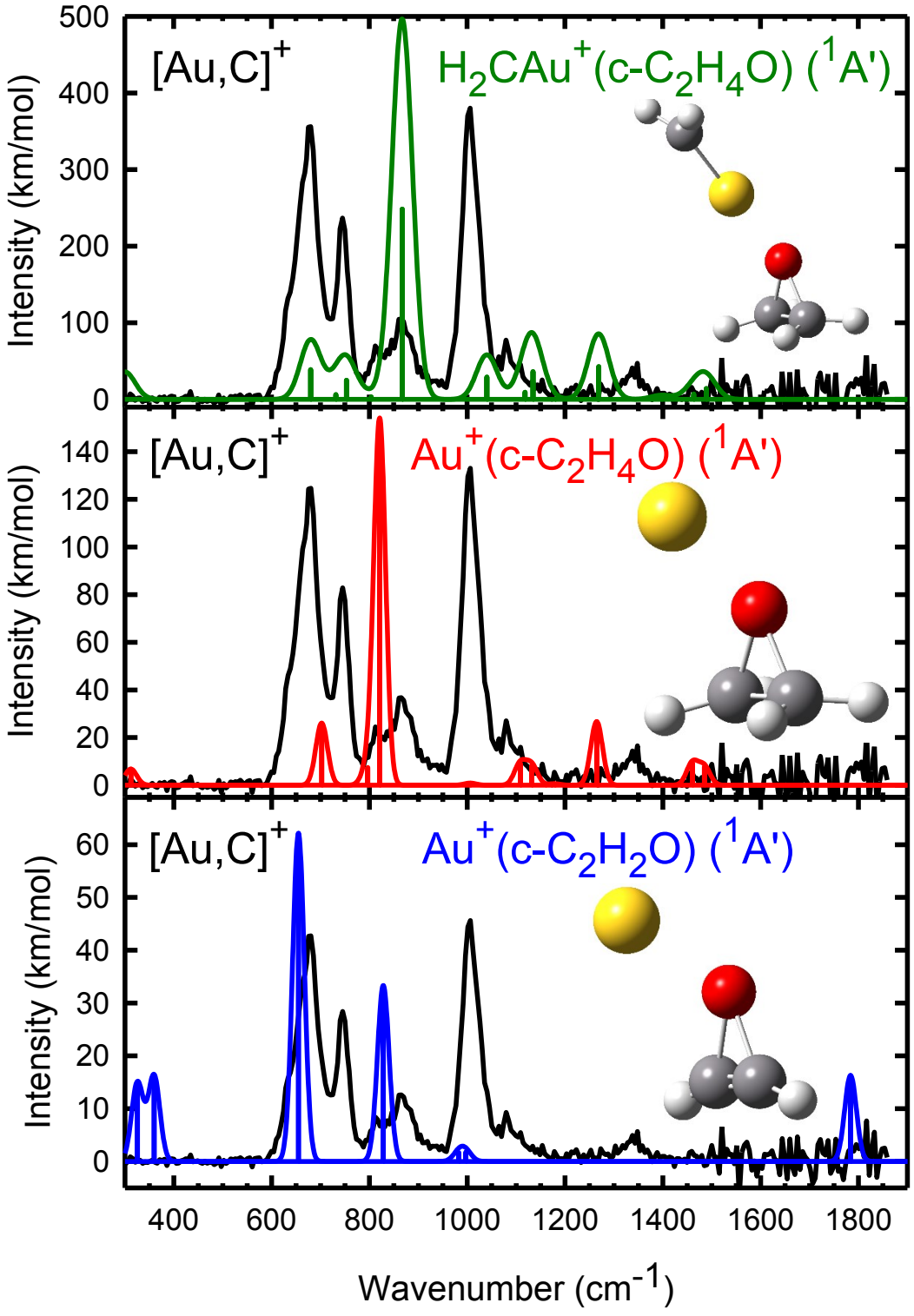
[Au,C]+
H2CAu+(c-C2H4O) (1A')
Intensity (km/mol)
[Au,C]+
Au+(c-C2H4O) (1A')
Intensity (km/mol)
[Au,C]+
Au+(c-C2H2O) (1A')
Intensity (km/mol)
Wavenumber (cm-1)

Figure 3

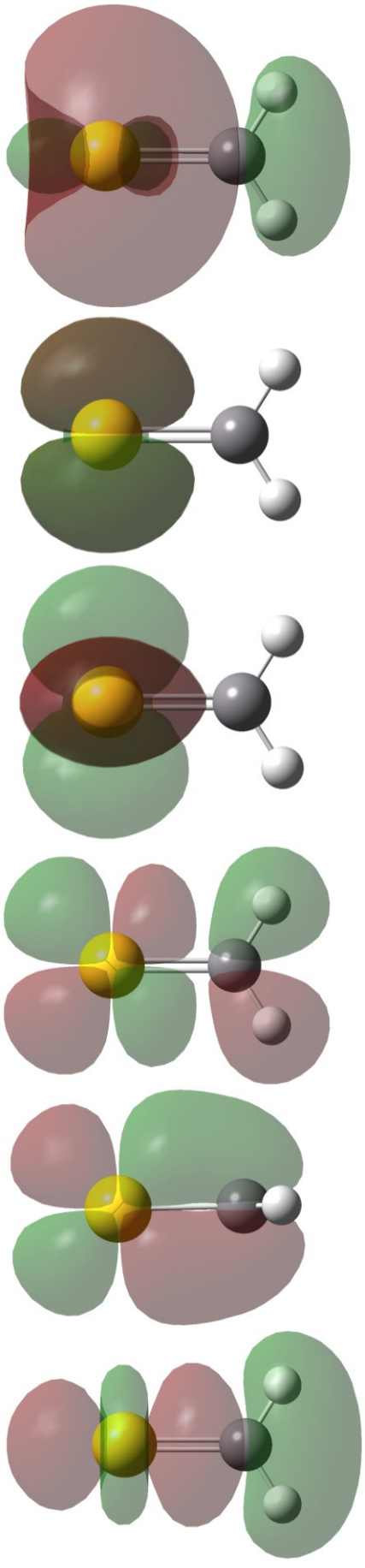

Figure 4

Table of Contents Graphic